

1 Multivalency drives the neutralizing activity of antibodies against the
2 *Plasmodium falciparum* circumsporozoite protein

3

4 Short Title: Antibody responses to the *Plasmodium* circumsporozoite protein

5

6 Camilla R. Fisher^{1¶}, Joe A. Kaczmarek^{1¶}, Henry J. Sutton^{2¶}, Ben Clifton¹, Joshua
7 Mitchell¹, Yeping Cai², Johanna N. Dups², Nicholas J. D'Arcy², Mandeep Singh²,
8 Hayley A. McNamara², Aaron Chuah², Tom Peat³, Colin J. Jackson^{1*} and Ian A.
9 Cockburn^{2*}

10

11 1. Research School of Chemistry, The Australian National University, Canberra, ACT
12 2601, Australia

13

14 2. John Curtin School of Medical Research, The Australian National University,
15 Canberra, ACT 2601, Australia

16

17 3. CSIRO Materials, Science and Engineering, Parkville, Victoria, Australia

18

19 * Corresponding authors

20 E-mail: colin.jackson@anu.edu.au

21 E-mail: ian.cockburn@anu.edu.au (lead contact).

22

23 ¶ These authors contributed equally to this work

24

25

26 **Abstract**

27

28 The repeat region of the *Plasmodium falciparum* circumsporozoite protein (CSP) is a
29 major vaccine antigen because it can be targeted by parasite neutralizing antibodies;
30 however, little is known about this interaction. We used isothermal calorimetry and
31 X-ray crystallography to analyze the binding of the *Plasmodium*-neutralizing 2A10
32 antibody to CSP. Strikingly, we found that the repeat region of CSP is bound by
33 multiple antibodies and that this multivalent interaction drives the affinity of this
34 antibody. Because the CSP protein can cross-link multiple B cell receptors (BCRs) we
35 hypothesized that the B cell response might be T-independent. However, by
36 sequencing the BCRs of CSP-repeat specific cells we found that these cells underwent
37 somatic hypermutation and affinity maturation indicative of a T-dependent response.
38 Interestingly, the BCR repertoire of responding B cells was limited suggesting that the
39 structural simplicity of the repeat may limit the breadth of the immune response.

40

41

42 **Author Summary**

43

44 Vaccines aim to protect by inducing the immune system to make molecules called
45 antibodies that can recognize molecules on the surface of invading pathogens. In the
46 case of malaria, our most advanced vaccine candidates aim to make antibodies that
47 recognize the circumsporozoite protein molecule on the surface of the invasive
48 parasite stage called the sporozoite. In this report we use X-ray crystallography to
49 determine the structure of CSP-binding antibodies at the atomic level. We use other
50 techniques such as isothermal titration calorimetry to examine how this antibody
51 interacts with the CSP molecule. Strikingly, we found that each CSP molecule could
52 bind 6 antibodies. This finding has implications for the immune response and may
53 explain why high titers of antibody are needed for protection. Moreover because the
54 structure of the CSP repeat is quite simple we determined that the number of different
55 kinds of antibodies that could bind this molecule are quite small. However those
56 antibodies can become quite high affinity as a result of a process called affinity
57 maturation that allows the body to learn how to make improved antibodies specific for
58 pathogen molecules. These data show that while it is challenging for the immune
59 system to recognize and neutralize CSP, it should be possible to generate viable
60 vaccines targeting this molecule.

61

62 **Introduction**

63

64 Malaria caused by *Plasmodium falciparum* causes the deaths of around
65 430,000 people each year [1]. The most advanced vaccine candidate is currently the
66 RTS,S/AS01 vaccine which consists of a truncated version of the sporozoite-surface
67 circumsporozoite protein (CSP), packaged in a Hepatitis C core virus-like particle
68 delivered in AS01 - a proprietary liposome based vaccine [2]. Phase II and Phase III
69 clinical trials have repeatedly demonstrated that the vaccine is capable of giving
70 around 50% protection against clinical malaria in field settings for the first year
71 following vaccination [3]. The bulk of protection is attributed to antibodies targeting
72 the CSP repeat epitope included within the vaccine, with some contribution from
73 CD4+ T cells [4]. It is still unclear why the antibody response to CSP is only partially
74 protective. We lack structural information about how neutralizing antibodies bind to
75 CSP and knowledge on the breadth and nature of the B cell response elicited.

76

77 Antibodies to CSP were first identified as potential mediators of protection
78 following seminal studies that showed that immunization with irradiated sporozoites
79 could induce sterile protection against live parasite challenge [5,6]. In the early 1980s,
80 monoclonal antibodies (mAbs) isolated from mice immunized with sporozoites were
81 found to be capable of inducing the neutralization of sporozoites (known as the
82 circumsporozoite reaction) and were used to clone CSP, one of the first malaria
83 antigens identified [7,8]. In all *Plasmodium* species CSP contains 3 domains: an N-
84 terminal domain and a C-terminal domain, separated by a repeat region, which was
85 the target of all the original mAbs identified [7,9,10]. In the 3D7 reference strain of *P.*
86 *falciparum* the CSP repeat has 38 NANP-repeats interspersed with 4 NVDP repeats

87 especially towards the N-terminus [11] though different numbers of repeats have been
88 observed [12]. One of the most effective *P. falciparum* sporozoite neutralizing
89 antibodies identified in these early studies was 2A10 which can neutralize sporozoite
90 infectivity *in vitro* [13] and in *in vivo* mouse models utilizing rodent *P. berghei*
91 parasites expressing the *P. falciparum* CSP repeat region [14,15].

92
93 While CSP binding antibodies have been shown to be able to neutralize
94 sporozoites and block infection, it has also been proposed that CSP is an
95 immunological “decoy” that induces a suboptimal T-independent immune response
96 perhaps because of the CSP repeat cross-linking multiple B cell receptors (BCRs)
97 [16]. Nonetheless this hypothesis has not been tested and it remains unknown if the
98 repetitive regions of CSP can cross-link multiple BCRs as they are not as large as
99 typical type-II T-independent antigens [17]. Furthermore, the very little published
100 data on the sequences of CSP binding antibodies does not convincingly support
101 activation of a broad B cell repertoire: a small study of five *P. falciparum* CSP mouse
102 monoclonal antibodies (mAbs) identified some shared sequences [18]. In humans, a
103 study that generated mAbs from three individuals who received RTS,S found that the
104 three antibodies studied had distinct sequences though these all used similar heavy
105 chains [19].

106
107 Given these gaps in our understanding of the antibody response to CSP we
108 undertook a comprehensive biophysical characterization of the 2A10 sporozoite-
109 neutralizing antibody that binds to the CSP repeat. Using rigorous biophysical
110 methodology we found that this antibody binds with a higher affinity than expected,
111 in the nano-molar range. Previous studies using competition ELISAs with peptides

112 predicted a micro-molar affinity [20,21]. Strikingly, isothermal titration calorimetry
113 and structural analyses revealed that the CSP repeat can be bound by around six
114 antibodies suggesting that it may require large amounts of antibody for neutralization,
115 and that the repeat may potentially crosslink multiple BCRs on the surface of a B cell.
116 However, analysis of CSP-specific B cells revealed that CSP-specific B cells can
117 enter germinal centers and undergo affinity maturation contradicting the notion that
118 the response to CSP is largely T-independent. Moreover, we found that the BCR
119 repertoire of CSP-binding B cells is quite limited which may restrict the size and
120 effectiveness of the immune response.

121 **Results**

122

123 **Characterization of the thermodynamics of 2A10-antigen binding**

124

125 We began our analysis by performing isothermal titration calorimetry (ITC) to
126 understand the interaction between 2A10 and CSP. For ease of expression we used a
127 recombinant CSP (rCSP) construct described previously which was slightly truncated
128 with 27 repeats [22]. ITC experiments were run on the purified 2A10 antibody and the
129 purified 2A10 antigen-binding fragment (F_{AB}) fragment to test the thermodynamic
130 basis of the affinity of 2A10 F_{AB} towards CSP. Experiments were also performed on
131 the 2A10 F_{AB} fragment with the synthetic peptide antigen (NANP)₆, which is a short
132 segment of the antigenic NANP-repeat region of CSP (**Table 1; Fig. 1**). The binding
133 free energies (ΔG) and dissociation constants (K_D) were found to be -49.0 kJ/mol and
134 2.7 nM for the full 2A10 antibody with CSP, -40 kJ/mol and 94 nM for the 2A10 F_{AB}
135 with CSP, and -36.4 kJ/mol and 420 nM for the 2A10 F_{AB} with the (NANP)₆ peptide.

136 Surprisingly, we did not observe a typical 1:1 antibody/ F_{AB} domain:antigen
137 binding stoichiometry (Table 1). We found that each (NANP)₆ peptide was bound to
138 by ~2 F_{AB} fragments (2.8 repeats per F_{AB} domain). With the rCSP protein we
139 observed that 10.8 ± 0.7 F_{AB} fragments were able to bind to each rCSP molecule, (2.5
140 repeats per F_{AB} domain. Finally, when the single-domain F_{AB} fragment is replaced by
141 the full 2A10 antibody (which has two F_{AB} domains), we observe binding of 5.8
142 antibodies per rCSP molecule (4.7 repeats per antibody), i.e. all complexes exhibit
143 approximately the same binding stoichiometry of two F_{AB} fragments/domains per ~5
144 repeat units. These results suggest that the antigenic region of CSP constitutes a
145 multivalent antigen and that repeating, essentially identical, epitopes must be

146 available for the binding of multiple F_{AB} domains.

147 It is not possible to separate affinity from avidity in this system, although it is
148 apparent that there is a substantial benefit to the overall strength of binding between
149 the antibody and antigen through the binding of multiple F_{AB} domains. The F_{AB} :rCSP
150 complex and the 2A10:rCSP complex had similar enthalpy and entropy of binding
151 (**Table 1**), but the lower enthalpy of binding for the F_{AB} fragment:(NANP)₆ peptide
152 complex suggests that there are additional stabilizing interactions when larger
153 numbers of F_{AB} domains can bind to the rCSP protein. The observation that this
154 antibody-antigen (Ab-Ag) interaction is primarily enthalpically driven is consistent
155 with the general mechanism of Ab-Ag interactions [23]. Altogether, these data
156 suggest that the binding of multiple antibodies to the repeat region of CSP stabilizes
157 the interaction and the multivalent nature of this interaction increases the affinity of
158 binding.

159

160 **Table 1. Thermodynamic parameters for interactions between 2A10 F_{AB} , 2A10**
161 **and antigens.**

	(NANP) ₆ : F_{AB}	rCSP: F_{AB}	rCSP:2A10
K_a (M^{-1})	$(2.37 \pm 0.91) \times 10^6$	$(1.07 \pm 0.39) \times 10^7$	$(3.6 \pm 2.7) \times 10^8$
K_d (nM)	420 ± 160	94 ± 34	2.7 ± 2.1
ΔH (kJ/mol complex)	-113 ± 5	-1245 ± 112	-1175 ± 44
$T\Delta S$ (kJ/mol complex)	-76.6 ± 4.9	-1205 ± 112	-1126 ± 44
ΔG (kJ/mol complex)	-36.4 ± 1.0	-40.0 ± 0.9	-49.0 ± 1.9
n (F_{AB} /2A10: Ag)	2.16 ± 0.06	10.8 ± 0.7	5.8 ± 0.1

162 Parameters were determined by ITC at 25 °C. Errors for n (Ag : F_{AB}), K_a and
163 ΔH (complex) are 95% confidence intervals estimated from a single titration; errors
164 for other parameters were propagated.

165

166 **Structural analysis of the (NANP)-repeat region and the 2A10 F_{AB}**

167

168 To better understand the molecular basis of the multivalent interaction
169 between 2A10 and rCSP, we performed structural analysis of the components.
170 Previous work has indicated that the NANP-repeat region of CSP adopts a flexible
171 rod-like structure with a regular repeating helical motif that provides significant
172 separation between the N-terminal and the C-terminal domains [24]. Here, we
173 performed far-UV circular dichroism (CD) spectroscopy to investigate the structure of
174 the (NANP)₆ peptide. These results were inconsistent with a disordered random coil
175 structure (**S1 Fig.**). Rather, the absorption maximum around 185 nm, minimum
176 around 202 nm and shoulder between 215 and 240 nm, is characteristic of intrinsically
177 disordered proteins that can adopt a spectrum of states [25].

178

179 The lowest energy structures of the (NANP)₆ repeat were predicted using the
180 PEP-FOLD *de novo* peptide structure prediction algorithm [26]. The only extended
181 state among the lowest energy structures that was consistent with the reported spacing
182 of the N-and C-terminal domains of CSP [24], and which presented multiple
183 structurally similar epitopes was a linear, quasi-helical structure, which formed a
184 regularly repeating arrangement of proline turns (**Fig. 2A**). The theoretical CD
185 spectrum of this conformation was calculated (**S1 Fig.**), qualitatively matching the
186 experimental spectra: the maximum was at 188 nm, the minimum at 203 nm and there
187 was a broad shoulder between 215 and 240 nm. To investigate the stability of this
188 conformation, we performed a molecular dynamics (MD) simulation on this peptide,
189 which showed that this helical structure could unfold, and refold, on timescales of

190 tens of nanoseconds, supporting the idea that it is a low-energy, frequently sampled,
191 configuration in solution (**S1 Mov.**, **S2 Fig.**). We also observed the same
192 characteristic hydrogen bonds between a carbonyl following the proline and the amide
193 nitrogen of the alanine, and the carbonyl group of an asparagine and a backbone
194 amide of asparagine three residues earlier, that are observed in the crystal structure of
195 the NPNA fragment [27]. Thus, this configuration, which is consistent with
196 previously published experimental data, is a regular, repeating, extended
197 conformation that would allow binding of multiple F_{AB} domains to several
198 structurally similar epitopes.

199

200 To better understand the interaction between the 2A10 and the (NANP)-repeat
201 region, we solved the crystal structure of the 2A10 F_{AB} fragment in two conditions (**S1**
202 **Table**), yielding structures that diffracted to 2.5 Å and 3.0 Å. All of the polypeptide
203 chains were modeled in good quality electron density maps (**Fig. 2B**), except for
204 residues 134-137 of the light chain. This loop is located at the opposite end of the F_{AB}
205 fragment to the variable region and not directly relevant to antigen binding. The 2.5 Å
206 structure contained a single polypeptide in the asymmetric unit, whereas the 3.0 Å
207 structure contained three essentially identical chains. Superimposition of the four
208 unique F_{AB} fragments from the two structures revealed that the variable antigen
209 binding region is structurally homogeneous, suggesting that this region might be
210 relatively pre-organized in the 2A10 F_{AB}. This is consistent with the observation that
211 antibodies typically undergo relatively limited conformational change upon epitope
212 binding [23]. Indeed, a recent survey of 49 antibody:antigen complexes revealed that
213 within the binding site, CDR-H3 was the only element that showed significant
214 conformational change upon antigen binding and even this was only observed in one

215 third of the antibodies [28].

216

217 Attempts to obtain a crystal structure of a complex between 2A10 F_{AB} and the
218 (NANP)₆ peptide were unsuccessful; unlike binary Ab-Ag interactions, in which the
219 Ab will bind to a single epitope on an antigen and produce a population of structurally
220 homogeneous complexes that can be crystallized, in this interaction we are dealing
221 with an intrinsically-disordered peptide, the presence of multiple binding sites
222 (epitopes) on the peptide and the possibility that more than one 2A10 F_{AB} domain can
223 bind the peptide, i.e. it is difficult to obtain a homogeneous population of complexes,
224 which is a prerequisite for crystallization. Attempts to soak the (NANP)₆ peptide into
225 the high-solvent form of 2A10 F_{AB}, in which there were no crystal packing
226 interactions with the binding-loops, caused the crystals to dissolve, again suggesting
227 that the heterogeneity of the peptide and the presence of multiple epitopes produces
228 disorder that is incompatible with crystal formation.

229

230 **Modeling the interaction of the 2A10 F_{AB} with the NANP-repeat region and**
231 **testing the model through site-directed mutagenesis**

232

233 Although it was not possible to obtain a crystal structure of the 2A10-
234 (NANP)₆ peptide complex, the accurate structures of the 2A10 F_{AB} fragment, the
235 (NANP)₆ peptide, and the knowledge that antibodies seldom undergo significant
236 conformational changes upon antigen binding [28], allowed us to model the
237 interaction, which we tested using site directed mutagenesis. Computational modeling
238 of Ab-Ag interactions has advanced considerably in recent years and several
239 examples of complexes with close to atomic accuracy have been reported in the

240 literature [29]. Using the SnugDock protein-protein docking algorithm [29], we
241 obtained an initial model for binding of the peptide to the CDR region of the 2A10
242 F_{AB} fragment (**Fig. 2C**). We then performed, in triplicate, three 50 ns molecular
243 dynamics simulations on this complex to investigate whether the interaction was
244 stable over such a time period (**S2 Mov.**, **S3 Fig.**). These simulations confirmed that
245 the binding mode that was modeled is stable, suggesting that it is a reasonable
246 approximation of the interaction between these molecules. To experimentally verify
247 whether our model of the 2A10 F_{AB}:(NANP)₆ peptide interaction was plausible, we
248 performed site directed mutagenesis of residues predicted to be important for binding.
249 Our model predicted that the interaction with (NANP)₆ would be mainly between
250 CDR2 and CDR3 of the light chain and CDR2 and CDR3 of the heavy chain (**Fig.**
251 **2C**).

252

253 In the light chain (**Fig. 3A,B**), Y38 is predicted to be one of the most
254 important residues in the interaction; it contributes to the formation of a hydrophobic
255 pocket that buries a proline residue and is within hydrogen bonding distance, *via* its
256 hydroxyl group, to a number of backbone and side-chain groups of the peptide. Loss
257 of this side-chain abolished binding. Y56 also forms part of the same proline-binding
258 pocket as Y38, and loss of this side-chain also resulted in an almost complete loss of
259 binding. R109 forms a hydrogen bond to an asparagine residue on the side of the
260 helix; mutation of this residue to alanine results in a partial loss of binding. Y116 is
261 located at the center of the second proline-binding pocket; since loss of the entire
262 side-chain through an alanine mutation would lead to general structural disruption of
263 the F_{AB} fragment, we mutated this to a phenylalanine (removing the hydroxyl group),
264 which led to a significant reduction in binding. Finally, S36A was selected as a

265 control: the model indicated that it was outside the binding site, and the ELISA data
266 indicated that had no effect on (NANP)_n binding.

267

268 Within the heavy chain (**Fig. 3C,D**), mutation of N57 to alanine led to
269 complete loss of binding, which is consistent with it forming a hydrogen bond to a
270 side-chain asparagine but also being part of a relatively well packed region of the
271 binding site that is mostly buried upon binding. T66 is located on the edge of the
272 binding site and appears to provide hydrophobic contacts through its methyl group
273 with the methyl side-chain of an alanine of the peptide; mutation of this residue
274 resulted in a partial loss of binding. Interestingly, mutation of E64, which is location
275 in an appropriate position to form some hydrogen bonds to the peptide resulted in a
276 slight increase in binding, although charged residues on the edge of protein:protein
277 interfaces are known to contribute primarily to specificity rather than affinity [30].
278 Specifically, the cost of desolvating charged residues such as glutamate is not
279 compensated for by the hydrogen bonds that may be formed with the binding partner.
280 Y37 is located outside the direct binding site in the apo-crystal structure; the loss of
281 affinity could arise from long-range effects, such as destabilization of the position of
282 nearby loops. In general, the effects of the mutations are consistent with the model of
283 the interaction.

284

285 **The multivalency of the CSP repeat region**

286

287 As shown in **Fig. 3A** and **3C** the binding mode of the F_{AB} fragment to the
288 (NANP)₆ peptide is centered on two proline residues from two non-adjacent NANP-
289 repeats. These cyclic side-chains are hydrophobic in character and are buried deeply

290 in the core of the F_{AB} antigen binding site, into hydrophobic pockets formed by Tyr38
291 and Tyr56 of the light chain and the interface between the two chains. In contrast, the
292 polar asparagine residues on the sides of the helix are involved in hydrogen binding
293 interactions with a number of polar residues on the edge of the binding site, such as
294 N57 of the heavy chain. Due to the twisting of the (NANP)₆ repeat, the binding
295 epitope of the peptide is 2.5-3 alternate NANP repeats, with a symmetrical epitope
296 available for binding on the opposite face (**Fig. 4A**). Thus, this binding mode is
297 consistent with the stoichiometry of the binding observed in the ITC measurements,
298 where we observed a stoichiometry of two 2A10 F_{AB} fragments per (NANP)₆ peptide.
299 To investigate whether this binding mode was also compatible with the indication
300 from ITC that ~10.7 2A10 F_{AB} fragments, or six antibodies (containing 12 F_{AB}
301 domains) could bind the CSP protein (**Table 1**), we extended the peptide to its full
302 length. It is notable that the slight twist in the NANP helix results in the epitope being
303 offset along the length of the repeat region, thereby allowing binding of ten 2A10 F_{AB}
304 fragments (**Fig. 4B**). Six 2A10 antibodies can bind if two antibodies interact by a
305 single F_{AB} domain and the other four interact with both F_{AB} domains. The observation
306 that the F_{AB} fragments bind sufficiently close to each other to form hydrogen bonds
307 also explains the observation from the ITC that the complexes with rCSP, which
308 allow adjacent F_{AB} fragment binding, have more favorable binding enthalpy, i.e. the
309 additional bonds formed between adjacent F_{AB} fragments further stabilize the
310 complex and lead to greater affinity (**Table 1**). Thus, the initially surprising
311 stoichiometry that we observe through ITC appears to be quite feasible based in the
312 structure of the NANP-repeat region of the rCSP protein and the nature of the rCSP-
313 2A10 complex. It is also clear that the effect of antibody binding to this region would
314 be to prevent the linker flexing between the N- and C-terminal domains and

315 maintaining normal physiological function, explaining the neutralizing effect of the
316 antibodies.

317

318 **Identification of endogenous (NANP)_n specific B cells to determine the BCR**
319 **repertoire**

320

321 We next set out to determine the implications of our structure for the B cell
322 response to CSP. In particular we wanted to know if the repeat structure drove a
323 diverse T-independent response resulting in a broad antibody response or if B cells
324 specific for CSP were able to enter the germinal center and undergo affinity
325 maturation. To test this hypothesis we used (NANP)_n-based tetramers to identify
326 antigen specific B cells in BALB/C mice immunized with *P. berghei* sporozoites
327 expressing the repeat region of the *P. falciparum* CSP (*P. berghei* CS^{Pf}) [15]. We then
328 used high throughput BCR sequencing to identify the BCR sequences of the (NANP)_n
329 specific cells. The tetramers are formed by the binding of 4 biotinylated (NANP)₉
330 repeats with streptavidin conjugated phycoerythrin (PE) or allophycocyanin (APC).
331 We used BALB/C mice as this was the strain originally used to generate 2A10. To
332 validate our tetramer approach, mice were immunized with either *P. berghei* CS^{Pf} or
333 another line of *P. berghei* with a mutant CSP (*P. berghei* CS^{5M}) that contains the
334 endogenous (*P. berghei*) repeat region, which has a distinct repeat sequence
335 (PPPPNPND)_n. (NANP)_n-specific cells were identified with two tetramer probes
336 bound to different conjugates to exclude B cells that are specific for the PE or APC
337 components of the tetramers which are numerous in mice [31]. We found that mice
338 immunized with *P. berghei* CS^{Pf} sporozoites developed large tetramer double positive
339 populations, which had class switched (**Fig. 5A and B**). In contrast, the number of

340 tetramer double positive cells in mice receiving control parasites was the same as in
341 unimmunized mice; moreover these cells were not class switched and appeared to be
342 naïve precursors indicating that our tetramers are identifying bona-fide (NANP)_n-
343 specific cells (**Fig. 5B** and **C**). Further analysis of the different populations of B cells
344 showed that most B cells present at this time-point were GL7⁺ CD38⁻ indicating that
345 they are germinal center B cells (**Fig. 5B** and **D**). Given that T cells are required to
346 sustain germinal center formation beyond ~3 days these data indicate that a T-
347 dependent response can develop to CSP following sporozoite immunization [32].

348

349 **A restricted repertoire of BCRs can bind to the (NANP)_n repeat**

350

351 We next set out to determine the diversity of the B cell response to CSP.
352 While the repeat structure of CSP is hypothesized to induce a broad polyclonal
353 response [33], an alternative hypothesis is that the antigenically simple structure of
354 the repeat epitope might only be recognized by a small number of naive B cells. To
355 examine the BCR usage of (NANP)_n-specific B cells we sorted (NANP)_n-specific
356 cells 35 days post immunization with sporozoites. We then prepared cDNA from the
357 cells and amplified the heavy and kappa chain sequences using degenerate primers as
358 described previously [34,35]. Heavy and light chain libraries were prepared from 4
359 immunized mice as well as from 3 naïve mice from which we bulk sorted B cells as
360 controls. We obtained usable sequences from 3 of the 4 mice for both the heavy chain
361 and kappa chain. Analysis of the heavy chain revealed that in each mouse 3 or 4 V
362 regions dominated the immune response (**Fig. 6A**). The V regions identified (IGHV1-
363 20; IGHV1-26; IGHV1-34 and IGHV5-9) were generally shared among the mice. As
364 a formal measure of the diversity of our V region usage in the (NANP)_n specific cells

365 and the bulk B cells from naïve mice we calculated the Shannon entropy for these
366 populations. This analysis formally demonstrated that the diversity of the antigen
367 specific B cells was significantly lower than the diversity of the repertoire in naïve
368 mice (**Fig. 6B**). We further found that each V region was typically associated with the
369 same D and J sequences even in different mice. For example, IGHV1-20 was
370 typically associated with J4, IGHV5-9 with J4 while in different mice IGHV1-34 was
371 variously paired with J1 or J4 (**Fig. 6C**). Similar results were obtained for the kappa
372 chain with the response dominated by IGKV1-135; IGKV5-43/45; IGKV1-110;
373 IGKV1-117 and IGKV14-111 (**Fig. 6D and E**). The V regions were typically paired
374 with the same J regions even in different mice (**Fig. 6F**), for example IGKV5.43/45
375 was typically paired with IGKJ5 or IGKJ2 and IGKV1-110 was typically paired with
376 IGKJ5, although IGKV1-135 was typically more promiscuous. One limitation of our
377 high throughput sequencing approach is that the degenerate primers only amplified
378 ~70% of the known IGHV and IGKV sequences in naïve mice, suggesting that we
379 may not capture the full diversity of the response. However, comparison with the 5
380 published antibody sequences (**S2 and S3 Table**) that include IGHV-1-20, IGKV5-45
381 and IGKV1-110 reveals that we are likely capturing the bulk of the antibody diversity.
382 Together these data suggest that the number of B cell clones responding to CSP may
383 be limited, potentially reducing the ability of the immune system to generate effective
384 neutralizing antibodies.

385

386 **CSP-binding antibodies undergo somatic hypermutation to improve affinity**

387

388 While it is clear that CSP is the target of neutralizing antibodies it has been
389 suggested that CSP might induce large T-independent responses at the expense of

390 potentially more useful T-dependent germinal center responses that can result in
391 robust B cell memory [33]. We therefore examined our deep sequencing data to
392 determine if CSP-specific antibodies had undergone somatic hypermutation (SHM)
393 that would be indicative of B cells specific for CSP entering the germinal center.
394 Taking advantage of the fact that our kappa chain primers capture the entire V-J
395 sequences of the antibodies we sequenced we asked: 1) if the kappa chains shared
396 between immune animals differed from the germline (providing evidence of SHM)
397 and 2) if the mutations were conserved between different mice indicative of directed
398 selection. Analysis of the reads from the kappa chains of the three immune mice
399 showed that these had a much higher degree of mutation than bulk B cells from naïve
400 mice, demonstrating SHM in the CSP-specific antibodies (**Fig. 7A**). We further
401 examined each specific common kappa chain in turn (IGVK1-110; IGKV1-135;
402 IGVK5-53/54) comparing the sequences obtained from naïve B cells and (NANP)_n
403 specific cells in immune mice. This analysis showed that while, as expected,
404 sequences from naïve mice contained few mutations, the sequences from immune
405 mice had much higher levels of SHM. Importantly mutations were found to be
406 concentrated in the CDR loops, and were frequently shared by immunized mice
407 providing strong circumstantial evidence for affinity maturation (**Fig. 7B**; data for
408 IGVK1-110 only shown).

409

410 To directly test if CSP-binding antibodies undergo affinity maturation we
411 expressed the predicted germline precursor to the 2A10 antibody (2A10 gAb) in
412 HEK293T cells. We identified the predicted germline precursors of the 2A10 heavy
413 and light chains using the program V-quest (**Figs. S4** and **S5**). This analysis identified
414 the heavy chain as IGHV9-3; IGHD1-3; IGHJ4 and the light chain as IGKV10-

415 94;IGKJ2, with the monoclonal antibody carrying 6 mutations in the heavy chain and
416 7 in the light chain. The 2A10 gAb had considerably lower binding in ELISA assays
417 compared to the 2A10 mAb itself (**Fig. 7C**) indicative that affinity maturation has
418 taken place in this antibody. To determine the relative contribution of mutations in the
419 heavy and light chain to enhancing binding we also made hybrid antibodies consisting
420 of the mAb heavy chain and the gAb light chain and vice versa. Interestingly
421 mutations in the light chain were almost entirely sufficient to explain the enhanced
422 binding by the mAb compared to the gAb (**Fig. 7C**).

423

424 To identify the specific mutations that were important we introduced the
425 mutations individually into the gAb light chain construct. We prioritized mutations
426 that were shared with the 27E antibody which has previously been found to be
427 clonally related to 2A10 having been isolated from the same mouse and which shares
428 the same germline heavy and light chains as the 2A10 mAb [18]. We found that two
429 mutations (L114F and T117V) in the CDR3 of the light chain appeared to account for
430 most of the gain in binding (**Fig. 7C**). The effect of these antibodies appeared to be
431 additive rather than synergistic as revealed by experiments in which we introduced
432 these mutations simultaneously (**Fig. 7D**). A further mutation close to the light chain
433 CDR2 (H68Y) also caused a modest increase in binding. As expected mutations in the
434 heavy chains appeared generally less important for increasing binding though M39I,
435 N59I and T67F all gave modest increases in binding (**Fig. 7E**). Collectively our data
436 suggest that CSP repeat antibodies can undergo somatic hypermutation in germinal
437 centers resulting in affinity maturation, however the antibody response may be limited
438 by the number of naïve B cells that can recognize and respond to this antigen.

439

440 Discussion

441

442 Here we provide an analysis of the structure of a *Plasmodium falciparum*
443 sporozoite-neutralizing antibody (2A10). We further model the binding of this
444 antibody with its antigen target, the repeat region of CSP, and provide a
445 thermodynamic characterization of this interaction. Finally, we used novel tetramer
446 probes to identify and sort antigen specific B cells responding to sporozoite
447 immunization in order to measure the diversity and maturation of the antibody
448 response. We found that the avidity of 2A10 for the rCSP molecule was in the
449 nanomolar range, which was much higher than the affinity previously predicted from
450 competition ELISAs with small peptides [20,21]. This affinity is a consequence of the
451 multivalent nature of the interaction, with up to 6 antibodies being able to bind to each
452 rCSP molecule. To spatially accommodate this binding the antibodies must surround
453 the CSP in an off-set manner, which is possible due to the slight twist in the helical
454 structure that the CSP can adopt. It is notable that the twisted, repeating arrangement
455 of the CSP linker is the only structure that would allow binding in the stoichiometry
456 observed through the ITC. We further found that the diversity of the antibody
457 repertoire to the CSP repeat was limited, perhaps due to the relative simplicity of the
458 target epitope. However, these antibodies have undergone affinity maturation to
459 improve affinity, potentially allowing protective immune responses to develop.

460

461 Using ITC we determined the affinity of 2A10 for rCSP to be 2.7 nM, which
462 is not unusual for a mouse mAb. However it is a much higher affinity than that
463 predicted from competition ELISAs that predicted a micro-molar affinity [20,21].
464 However, these competition ELISAs were performed with short peptides rather than

465 rCSP. Indeed, when we performed ITC with a short peptide and F_{AB} fragments we too
466 obtained an affinity in the micro-molar range (0.42 μM). The difference in avidity
467 between the F_{AB} binding to the peptide or full-length CSP and that of the antibody
468 appears to be driven by a more favorable enthalpy of binding. It is likely that
469 additional stabilizing interactions between adjacent F_{AB} domains, which is consistent
470 with the structural model, contribute to this. One caveat of these data is that we used a
471 slightly truncated repeat, however it is likely that longer repeats will have further
472 stabilization of the interaction that could result in even higher affinity interaction
473 between CSP and binding antibodies.

474

475 Our data provide important insights into the requirements for sporozoite-
476 neutralization by CSP binding antibodies. The finding that each rCSP molecule can be
477 bound by ~ 6 antibody molecules is consistent with the finding that relatively large
478 amounts of antibody are required for protection against sporozoites [14,19,36].
479 Indeed, this may be an underestimate and it may be that full-length CSP can
480 accommodate additional antibody binding. If on the one hand, the surface of the
481 sporozoite provides multiple binding sites for CSP binding antibodies this may allow
482 the parasites to be relatively easily opsonized and phagocytized. On the other hand,
483 this may not be an important mechanism of action as anti-CSP F_{AB} fragments have
484 previously been shown to be sufficient for blocking sporozoite infectivity in vivo
485 [36]. Moreover CSP is readily shed from the surface of the sporozoite as the
486 sporozoites undergo migration, which may act as a means of sloughing off bound
487 antibody to evade this response [37]. It has also been suggested that the CSP repeat
488 might act as a hinge allowing the N-terminal domain to mask the C-terminal domain
489 that is believed to be important for binding to and invading hepatocytes [9]. Antibody

490 binding as observed here may disrupt this hinge perhaps resulting in the premature
491 exposure of the C-terminal domain and the loss of sporozoite infectivity.

492

493 Our results uncovering how neutralizing antibodies bind to CSP has several
494 implications for understanding the development of the immune response to CSP.
495 Notably the finding that the CSP molecule can be bound by multiple antibodies/B cell
496 receptors raises the possibility that this molecule can indeed crosslink multiple BCRs
497 and potentially act as a type-II T independent antigen [17]. Such antigens typically
498 induce large but relatively short-lived immune responses [17]. Interestingly, the
499 RTS,S/AS01 vaccine based on that contains 18 CSP repeats and does appear to induce
500 high, but relatively short-lived, titers of anti-CSP antibodies [4,38], which would be
501 consistent with it inducing a type-II T-independent response. Nonetheless, we also
502 detected extensive somatic hypermutation and affinity maturation, not only from
503 established monoclonal antibodies but also from CSP-specific B cells following a
504 single sporozoite immunization. Thus, there is a T-dependent germinal center
505 component to the antibody response too. The relative contributions of short-lived
506 antibody production and long-term B cell memory to protection is an area for future
507 investigation.

508

509 The finding of a limited repertoire in the BCR sequences specific for the
510 (NANP)_n repeat contradicts previous suggestions that the response to CSP might be
511 broad and polyclonal [33]. One explanation for this limited antibody diversity is that
512 the antigenic simplicity of the CSP repeat region limits the range of antibodies that are
513 capable of responding. A prior example of this is the antibodies to the Rhesus (Rh) D
514 antigen. The RhD antigen differs from RhC by only 35-36 amino acids, resulting in

515 the creation of a minimal B cell epitope [39]. The repertoire of antibodies that can
516 bind this epitope are accordingly limited and mainly based on the VH3-33 gene
517 family [40]. Another potential explanation for a limited antibody repertoire could be
518 that the (NANP)_n repeat shares structural similarity with a self-antigen as is
519 speculated to happen with meningococcus type B antigens [41], however it is not
520 clear what this self-antigen might be. One potential outcome of this finding is that if
521 each B cell clone has a finite burst size this may limit the magnitude of the overall B
522 cell response.

523

524 One area for future investigation is to determine the binding modes and
525 sporozoite neutralizing capacities of other antibodies in the response. It is clear that
526 not all CSP-repeat binding antibodies have the same capacity for sporozoite
527 neutralization [13]. As such the finding of a limited repertoire of responding B cells
528 may lead to the possibility that some people have holes in their antibody repertoires
529 limiting their ability to make neutralizing antibodies. This may explain why, while
530 there is a broad correlation between ELISA titres of antibodies to the CSP repeat and
531 protection following RTS,S vaccination, there is no clear threshold for protection [4].

532

533 While our work has been performed with mouse antibodies, there are major
534 similarities between mouse and human antibody loop structure [42]. The main
535 difference between the two species is the considerably more diverse heavy chain
536 CDR3 regions that are found in human antibodies [43]. In terms of our sequence data,
537 it may be that humans may have a more diverse antibody repertoire, not least because
538 as larger individuals they may have a greater diversity of naïve B cells specific CSP.
539 However, it is notable that all 4 human monoclonal antibodies described to date from

540 different volunteers share the use of the IGHV3-30 gene family [19,20], suggesting
541 that in humans as well as mice there is a constrained repertoire of responding B cells.

542

543 Overall our data provide important insights into how the antibody response to
544 CSP develops. Our results also help explain why relatively large amounts of
545 antibodies are required for sporozoite neutralization and suggest that the ability to
546 generate an effective B cell response may be limited by the very simplicity of the
547 repeat epitope. These data support previous suggestions that CSP may be a
548 suboptimal target for vaccination. However, we also find that CSP binding antibodies
549 can undergo somatic hypermutation and reach high affinities. This suggests if we can
550 develop vaccination strategies to diversify the repertoire of responding B cells and
551 favor the germinal center response it may be possible to generate long-term protective
552 immunity targeting this major vaccine candidate antigen.

553

554

555 **Methods**

556

557 **Ethics statement**

558 All animal procedures were approved by the Animal Experimentation Ethics
559 Committee of the Australian National University (Protocol numbers: A2013/12;
560 A2014/62 and A2015/76). All research involving animals was conducted in
561 accordance with the National Health and Medical Research Council's (NHMRC)
562 Australian Code for the Care and Use of Animals for Scientific Purposes and the
563 Australian Capital Territory Animal Welfare Act 1992.

564

565 **Mice and Immunizations**

566 BALB/C mice (bred in house at the Australian National University) were immunized
567 IV with 5×10^4 *P. berghei* CS^{5M} sporozoites expressing mCherry [44] or 5×10^4 *P.*
568 *berghei* CS^{Pf} sporozoites dissected by hand from the salivary glands of *Anopheles*
569 *stephensi* mosquitoes. Mice were then treated with 0.6mg chloroquine IP daily for 10
570 days to prevent the development of blood stage infection.

571

572 **Flow Cytometry and sorting**

573 Single cell preparations of lymphocytes were isolated from the spleen of immunized
574 mice and were stained for flow cytometry or sorting by standard procedures. Cells
575 were stained with lineage markers (anti-CD3, clone 17A2; anti-GR1, clone RB6-8C5
576 and anti-NKp46, clone 29A1.4) antibodies to B220 (clone RA3-6B2), IgM (clone
577 II/41), IgD (11-26c2a) and (NANP)₉ tetramers conjugated to PE or APC. Antibodies
578 were purchased from Biolegend while tetramers were prepared in house by mixing
579 biotinylated (NANP)₉ peptide with streptavidin conjugated PE or APC (Invitrogen) in

580 the a 4:1 molar ratio. Flow-cytometric data was collected on a BD Fortessa flow
581 cytometer (Becton Dickinson) and analyzed using FlowJo software (FlowJo). Where
582 necessary cells were sorted on a BD FACs Aria I or II machine.

583

584 **Sequencing of (NANP)_n specific cells and BCR analysis**

585 Single cell suspensions from the spleens of immunized mice were stained with
586 (NANP)_n tetramers and antibodies to B cell markers as described in the supplemental
587 experimental procedures. Antigen specific cells were sorted on a FACS ARIA I or II
588 instrument prior to RNA extraction with the Arturus Picopure RNA isolation kit
589 (Invitrogen) and cDNA preparation using the iScript cDNA synthesis kit (BioRad).
590 BCR sequences were amplified using previously described heavy and kappa chain
591 primers including adaptor sequences allowing subsequent indexing using the Nextera
592 indexing kit (Illumina). Analysis was performed in house using R-scripts and the
593 program MiXCR as described in supplemental experimental procedures.

594

595 **Binding of antibody variants**

596 Variants of the 2A10 antibody were expressed in HEK293 T cells (a kind gift of
597 Carola Vinuesa, Australian National University) as described in the supplemental
598 experimental procedures. Binding to the CSP repeat was tested by ELISA and ITC
599 using standard techniques as described in the supplemental experimental procedures.

600

601 **Data Deposition**

602 Sequence data generated in this paper is deposited at the NCBI BioProject database
603 accession number PRJNA352758. Atomic coordinates and related experimental data

604 for structural analyses are deposited in the Protein Data Bank (PDB) with PDB codes

605 5ZSF and 5TOY.

606 **Acknowledgments**

607

608 We thank the C3 Crystallisation Centre at CSIRO for help with crystal formation and
609 the Australian Synchrotron and beamline scientists for help with data collection. We
610 thank Michael Devoy, Harpreet Vohra and Catherine Gillespie of the Imaging and
611 Cytometry Facility at the John Curtin School of Medical Research for assistance with
612 flow cytometry and multi-photon microscopy.

613

614 **References**

615

616 1. World Health Organization (2016) World Malaria Report 2016. Geneva: World
617 Health Organization.

618 2. Casares S, Brumeanu TD, Richie TL (2010) The RTS,S malaria vaccine. *Vaccine*
619 28: 4880-4894.

620 3. RTS,S Clinical Trials Partnership (2015) Efficacy and safety of RTS,S/AS01
621 malaria vaccine with or without a booster dose in infants and children in
622 Africa: final results of a phase 3, individually randomised, controlled trial.
623 *Lancet* 386: 31-45.

624 4. White MT, Bejon P, Olotu A, Griffin JT, Riley EM, et al. (2013) The relationship
625 between RTS,S vaccine-induced antibodies, CD4(+) T cell responses and
626 protection against *Plasmodium falciparum* infection. *PLoS One* 8: e61395.

627 5. Nussenzweig RS, Vanderberg J, Most H, Orton C (1967) Protective immunity
628 produced by the injection of x-irradiated sporozoites of *plasmodium berghei*.
629 *Nature* 216: 160-162.

630 6. Seder RA, Chang LJ, Enama ME, Zephir KL, Sarwar UN, et al. (2013) Protection
631 against malaria by intravenous immunization with a nonreplicating sporozoite
632 vaccine. *Science* 341: 1359-1365.

633 7. Dame JB, Williams JL, McCutchan TF, Weber JL, Wirtz RA, et al. (1984)
634 Structure of the gene encoding the immunodominant surface antigen on the
635 sporozoite of the human malaria parasite *Plasmodium falciparum*. *Science*
636 225: 593-599.

- 637 8. Yoshida N, Nussenzweig RS, Potocnjak P, Nussenzweig V, Aikawa M (1980)
638 Hybridoma produces protective antibodies directed against the sporozoite
639 stage of malaria parasite. *Science* 207: 71-73.
- 640 9. Coppi A, Natarajan R, Pradel G, Bennett BL, James ER, et al. (2011) The malaria
641 circumsporozoite protein has two functional domains, each with distinct roles
642 as sporozoites journey from mosquito to mammalian host. *J Exp Med* 208:
643 341-356.
- 644 10. Zavala F, Cochrane AH, Nardin EH, Nussenzweig RS, Nussenzweig V (1983)
645 Circumsporozoite proteins of malaria parasites contain a single
646 immunodominant region with two or more identical epitopes. *J Exp Med* 157:
647 1947-1957.
- 648 11. Gardner MJ, Hall N, Fung E, White O, Berriman M, et al. (2002) Genome
649 sequence of the human malaria parasite *Plasmodium falciparum*. *Nature* 419:
650 498-511.
- 651 12. Zeeshan M, Alam MT, Vinayak S, Bora H, Tyagi RK, et al. (2012) Genetic
652 variation in the *Plasmodium falciparum* circumsporozoite protein in India and
653 its relevance to RTS,S malaria vaccine. *PLoS One* 7: e43430.
- 654 13. Hollingdale MR, Nardin EH, Tharavanij S, Schwartz AL, Nussenzweig RS (1984)
655 Inhibition of entry of *Plasmodium falciparum* and *P. vivax* sporozoites into
656 cultured cells; an in vitro assay of protective antibodies. *J Immunol* 132: 909-
657 913.
- 658 14. Espinosa DA, Gutierrez GM, Rojas-Lopez M, Noe AR, Shi L, et al. (2015)
659 Proteolytic Cleavage of the *Plasmodium falciparum* Circumsporozoite Protein
660 Is a Target of Protective Antibodies. *J Infect Dis* 212: 1111-1119.

- 661 15. Persson C, Oliveira GA, Sultan AA, Bhanot P, Nussenzweig V, et al. (2002)
662 Cutting edge: a new tool to evaluate human pre-erythrocytic malaria vaccines:
663 rodent parasites bearing a hybrid Plasmodium falciparum circumsporozoite
664 protein. *J Immunol* 169: 6681-6685.
- 665 16. Schofield L, Uadia P (1990) Lack of Ir-Gene Control in the Immune-Response to
666 Malaria .1. A Thymus-Independent Antibody-Response to the Repetitive
667 Surface Protein of Sporozoites. *Journal of Immunology* 144: 2781-2788.
- 668 17. Defrance T, Taillardet M, Genestier L (2011) T cell-independent B cell memory.
669 *Current Opinion in Immunology* 23: 330-336.
- 670 18. Anker R, Zavala F, Pollok BA (1990) VH and VL region structure of antibodies
671 that recognize the (NANP)₃ dodecapeptide sequence in the circumsporozoite
672 protein of Plasmodium falciparum. *Eur J Immunol* 20: 2757-2761.
- 673 19. Foquet L, Hermsen CC, van Gemert GJ, Van Braeckel E, Weening KE, et al.
674 (2014) Vaccine-induced monoclonal antibodies targeting circumsporozoite
675 protein prevent Plasmodium falciparum infection. *J Clin Invest* 124: 140-144.
- 676 20. Chappel JA, Rogers WO, Hoffman SL, Kang AS (2004) Molecular dissection of
677 the human antibody response to the structural repeat epitope of Plasmodium
678 falciparum sporozoite from a protected donor. *Malar J* 3: 28.
- 679 21. Zavala F, Tam JP, Hollingdale MR, Cochrane AH, Quakyi I, et al. (1985)
680 Rationale for development of a synthetic vaccine against Plasmodium
681 falciparum malaria. *Science* 228: 1436-1440.
- 682 22. Cerami C, Frevert U, Sinnis P, Takacs B, Clavijo P, et al. (1992) The basolateral
683 domain of the hepatocyte plasma membrane bears receptors for the
684 circumsporozoite protein of Plasmodium falciparum sporozoites. *Cell* 70:
685 1021-1033.

- 686 23. Braden BC, Poljak RJ (1995) Structural features of the reactions between
687 antibodies and protein antigens. *FASEB J* 9: 9-16.
- 688 24. Plassmeyer ML, Reiter K, Shimp RL, Jr., Kotova S, Smith PD, et al. (2009)
689 Structure of the *Plasmodium falciparum* circumsporozoite protein, a leading
690 malaria vaccine candidate. *J Biol Chem* 284: 26951-26963.
- 691 25. Kelly SM, Jess TJ, Price NC (2005) How to study proteins by circular dichroism.
692 *Biochim Biophys Acta* 1751: 119-139.
- 693 26. Shen Y, Maupetit J, Derreumaux P, Tuffery P (2014) Improved PEP-FOLD
694 Approach for Peptide and Miniprotein Structure Prediction. *J Chem Theory*
695 *Comput* 10: 4745-4758.
- 696 27. Ghasparian A, Moehle K, Linden A, Robinson JA (2006) Crystal structure of an
697 NPNA-repeat motif from the circumsporozoite protein of the malaria parasite
698 *Plasmodium falciparum*. *Chem Commun (Camb)*: 174-176.
- 699 28. Sela-Culang I, Alon S, Ofran Y (2012) A systematic comparison of free and
700 bound antibodies reveals binding-related conformational changes. *J Immunol*
701 189: 4890-4899.
- 702 29. Sircar A, Gray JJ (2010) SnugDock: paratope structural optimization during
703 antibody-antigen docking compensates for errors in antibody homology
704 models. *PLoS Comput Biol* 6: e1000644.
- 705 30. Davis SJ, Davies EA, Tucknott MG, Jones EY, van der Merwe PA (1998) The
706 role of charged residues mediating low affinity protein-protein recognition at
707 the cell surface by CD2. *Proc Natl Acad Sci U S A* 95: 5490-5494.
- 708 31. Pape KA, Taylor JJ, Maul RW, Gearhart PJ, Jenkins MK (2011) Different B cell
709 populations mediate early and late memory during an endogenous immune
710 response. *Science* 331: 1203-1207.

- 711 32. de Vinuesa CG, Cook MC, Ball J, Drew M, Sunners Y, et al. (2000) Germinal
712 centers without T cells. *J Exp Med* 191: 485-494.
- 713 33. Schofield L (1990) The circumsporozoite protein of Plasmodium: a mechanism of
714 immune evasion by the malaria parasite? *Bull World Health Organ* 68 Suppl:
715 66-73.
- 716 34. Arnaout R, Lee W, Cahill P, Honan T, Sparrow T, et al. (2011) High-resolution
717 description of antibody heavy-chain repertoires in humans. *PLoS One* 6:
718 e22365.
- 719 35. Busse CE, Czogiel I, Braun P, Arndt PF, Wardemann H (2014) Single-cell based
720 high-throughput sequencing of full-length immunoglobulin heavy and light
721 chain genes. *Eur J Immunol* 44: 597-603.
- 722 36. Potocnjak P, Yoshida N, Nussenzweig RS, Nussenzweig V (1980) Monovalent
723 fragments (Fab) of monoclonal antibodies to a sporozoite surface antigen
724 (Pb44) protect mice against malarial infection. *J Exp Med* 151: 1504-1513.
- 725 37. Stewart MJ, Vanderberg JP (1988) Malaria Sporozoites Leave Behind Trails of
726 Circumsporozoite Protein during Gliding Motility. *Journal of Protozoology*
727 35: 389-393.
- 728 38. White MT, Bejon P, Olotu A, Griffin JT, Bojang K, et al. (2014) A combined
729 analysis of immunogenicity, antibody kinetics and vaccine efficacy from
730 phase 2 trials of the RTS,S malaria vaccine. *BMC Med* 12: 117.
- 731 39. Avent ND, Madgett TE, Lee ZE, Head DJ, Maddocks DG, et al. (2006) Molecular
732 biology of Rh proteins and relevance to molecular medicine. *Expert Rev Mol*
733 *Med* 8: 1-20.

- 734 40. Chang TY, Siegel DL (1998) Genetic and immunological properties of phage-
735 displayed human anti-Rh(D) antibodies: implications for Rh(D) epitope
736 topology. *Blood* 91: 3066-3078.
- 737 41. Finne J, Leinonen M, Makela PH (1983) Antigenic similarities between brain
738 components and bacteria causing meningitis. Implications for vaccine
739 development and pathogenesis. *Lancet* 2: 355-357.
- 740 42. North B, Lehmann A, Dunbrack RL (2011) A New Clustering of Antibody CDR
741 Loop Conformations. *Journal of Molecular Biology* 406: 228-256.
- 742 43. Stanfield RL, Wilson IA (2014) Antibody Structure. *Microbiology spectrum* 2.
- 743 44. Cockburn IA, Tse SW, Zavala F (2014) CD8+ T cells eliminate liver stage
744 Plasmodium parasites without detectable bystander effect. *Infect Immun.*
745
746
747

748 **Supporting Information Legends**

749

750 **S1 Fig. Theoretical (A) and experimental (B) CD spectra of the (NANP)₆ peptide.**

751 The computational prediction of the spectra (A) was performed using DichroCalc [9],
752 the experimental spectra was measured at 222 nm at 25 °C. A peak at 185 nm,
753 minimum at 205 nm and shoulder between 215 and 240 nm are consistent with an
754 intrinsically disordered, but not random coil, structure.

755

756 **S2 Fig. Cluster analysis for MD simulations of (NANP)₆ peptide.** Conformations

757 were clustered by concatenating the trajectory and performing a Jarvis-Patrick
758 analysis. The clusters are sorted by their RMSD from the first cluster (starting
759 geometry). As shown, Run 2 is stable in the starting geometry for several ns, while
760 Run 3 diverged, then reconverged to the starting geometry, where it was stable for
761 several ns. These data suggest the quasi-helical structure observed from the ab initio
762 calculations is stable, and can be spontaneously sampled, on a timescale of several ns.

763

764 **S3 Fig. Cluster analysis for MD simulations of (NANP)₆ peptide.** Molecular

765 dynamics simulation of the (NANP)₆:F_{AB} complex. Root mean square deviation
766 (RMSD) of the (NANP)₆:F_{AB} complex as a function of time, independent simulations
767 are shown in green, black and red.

768

769 **S4 Fig: Alignment of 2A10 heavy chain and the predicted germline sequence**

770 Residues that are mutated away from the predicted germline sequence in more one or
771 more other antibody heavy chain (2E7 or 3D6) are highlighted in red, mutations that
772 are predicted to be involved in binding to CSP are highlighted in blue.

773

774 **S5 Fig: Alignment of 2A10 heavy chain and the predicted germline sequence**

775 Residues that are mutated away from the predicted germline sequence in both 2A10
776 and the related 2E7 antibody are highlighted in red, mutations that are predicted to be
777 involved in binding to CSP are highlighted in blue.

778

779 **Movie S1: Molecular Dynamics simulation of the solution structure of the**
780 **(NANP)₆ peptide**

781 Excerpt from (NANP)₆ run 3. Trajectory was fitted to minimize alpha-carbon RMSD
782 and then passed through a low-pass filter with filter length 8 frames to reduce
783 temporal aliasing.

784

785 **Movie S2: Molecular Dynamics simulation of the interaction of the (NANP)_n**
786 **repeat with the 2A10 FAB**

787 Excerpt from 2A10:(NANP)₆ run 3. Trajectory was fitted to minimize alpha-carbon
788 RMSD and then passed through a low-pass filter with filter length 8 frames to reduce
789 temporal aliasing.

790

791 **Figure Legends**

792

793 **Fig. 1. ITC data for interactions between 2A10 F_{AB} and antigens.** (A) Titration of
794 2A10 F_{AB} with (NANP)₆. (B) Titration of 2A10 F_{AB} with rCSP. (C) Titration of 2A10
795 with rCSP. The upper panels represent baseline-corrected power traces. By
796 convention, negative power corresponds to exothermic binding. The lower panels
797 represent the integrated heat data fitted to the independent binding sites model.

798

799 **Fig 2. Structures of the (NANP)₆ peptide (A), the 2A10 F_{AB} fragment (B) and the**
800 **model of the F_{AB} fragment-(NANP)₆ complex (C).** (A) The calculated structure of
801 the (NANP)₆ peptide is a helical structure containing the same hydrogen bonds
802 between a carbonyl following the proline and the amide nitrogen of the alanine, and
803 the carbonyl group of an asparagine and a backbone amide of asparagine 3 residues
804 earlier (highlighted in red) that are observed in [27]. (B) Electron density (blue mesh;
805 2mF_o-dF_c at 1 σ) of the 2A10 F_{AB} fragment viewed from above the antigen-binding
806 site. Light chain is shown as yellow sticks, heavy chain as cyan. (C) A calculated
807 model of the (NANP)₆:2A10 F_{AB} fragment complex. The CDR2 regions of each chain
808 are shown in red, the CDR3 regions of each chain are shown in blue.

809 **Fig 3. Detailed view of the (NANP)₆:2A10 F_{AB} interface and site directed**
810 **mutagenesis.** (A) A model of the light chain:(NANP)₆ interface. (B) ELISA results
811 showing the effect of mutating light chain interface residues; error bars are based on
812 technical replicates from one of two independent experiments. (C) A model of the
813 heavy chain:(NANP)₆ interface. (D) ELISA results showing the effect of mutating
814 heavy chain interface residues; error bars are based on technical replicates from one

815 of two independent experiments.

816 **Fig 4. The multivalency of the NANP repeat region of the CSP protein.** (A) An
817 (NANP)₆ peptide results in the presentation of two symmetrical epitopes, formed by
818 alternating repeats (cyan and magenta), allowing binding by two F_{AB} domains, in
819 keeping with the stoichiometry observed by ITC. (B) The full 27-mer repeat region
820 results in the presentation of at least 10 separate epitopes and the twist of the helix
821 results in displacement along the length of the repeat region, which allows binding of
822 up to 10 separate F_{AB} fragments, consistent with 4 antibodies bound by both F_{AB}
823 domains, and two bound by a single F_{AB} domain.

824

825 **Fig 5. CSP-specific B cells enter the germinal center following sporozoite**
826 **immunization.** BALB/C Mice were immunized with either 5×10^4 *P. berghei* CS^{5M}
827 (expressing the endogenous *P. berghei* CSP repeat) or 5×10^4 *P. berghei* CS^{Pf}
828 (expressing the circumsporozoite protein from *P. falciparum*). 12 days later the B cell
829 response was analyzed by flow cytometry and putative (NANP)_n-specific cells were
830 identified using PE and APC conjugated tetramers. (A) Representative flow
831 cytometry plots showing the identification of (NANP)_n-specific (Tetramer+) cells. (B)
832 Representative flow cytometry plots showing the proportion of Tetramer+ cells that
833 have class switched and entered a germinal center. (C) Quantification of the number
834 of class switched Tetramer+ cells under different immunization conditions. (D)
835 Quantification of the number of germinal center Tetramer+ cells under different
836 immunization conditions.

837

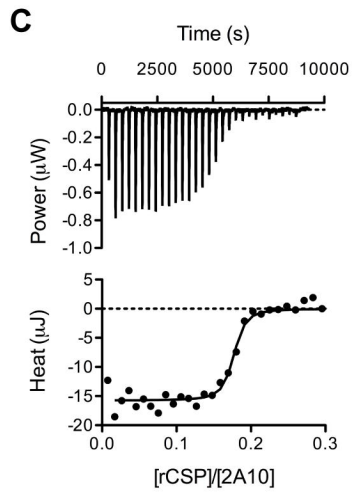
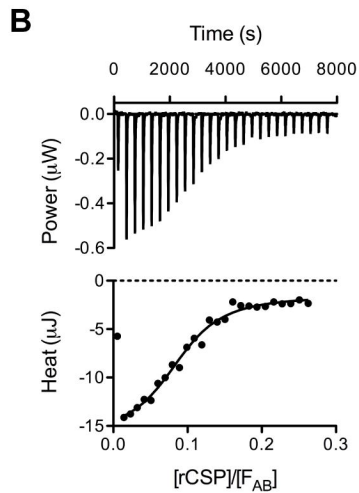
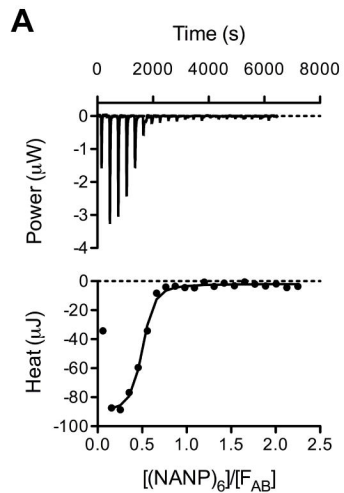
838 **Fig 6. Limited diversity of (NANP)_n specific antibodies.** BCR sequences were
839 amplified from Tetramer+ cells sorted from BALB/C mice 35 days after

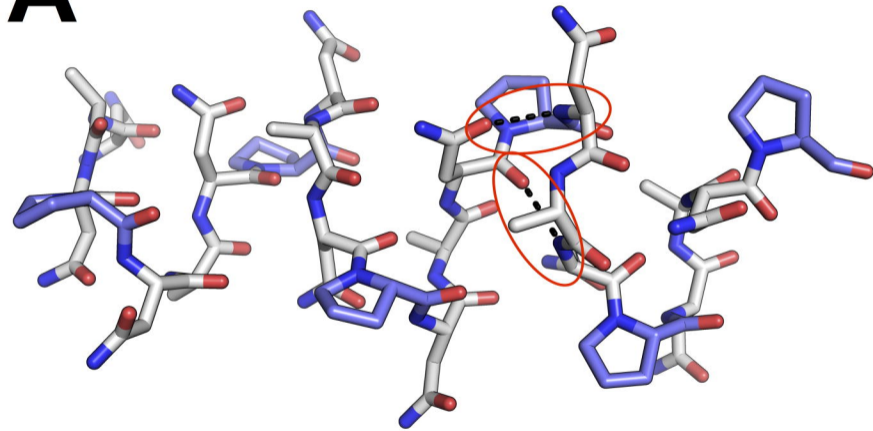
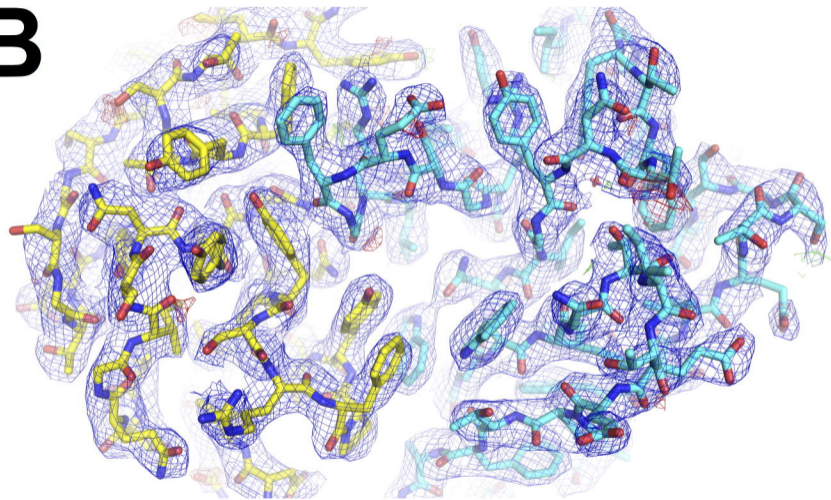
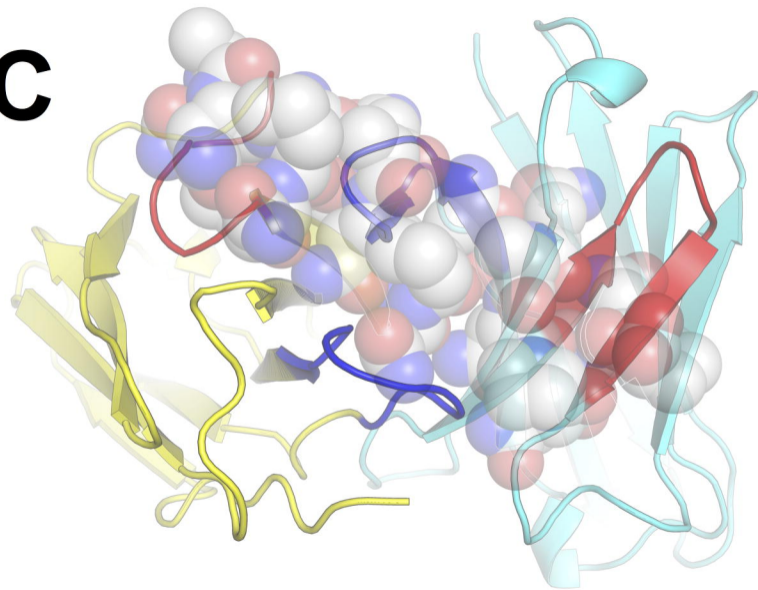
840 immunization with *P. berghei* CS^{Pf} as well as bulk B cells from naïve BALB/C mice
841 (A) IGHV gene usage from among B cells from a representative naïve mouse (grey
842 bars) and Tetramer+ cells from immune mice (red, blue and yellow bars). (B)
843 Shannon's diversity calculated for the diversity of IGHV region usage among bulk B
844 cells and Tetramer+ cells. (C) Circos plots showing the IGHV-IGHJ pairings in a
845 representative naïve mice and 3 immune mice. (D) IGKV gene usage from among B
846 cells from a representative naïve mouse (grey bars) and Tetramer+ cells from immune
847 mice (red, blue and green bars). (E) Shannon's diversity calculated for the diversity of
848 IGKV region usage among bulk B cells and Tetramer+ cells. (F) Circos plots showing
849 the IGKV-IGKJ pairings in a representative naïve mouse and 3 immune mice.

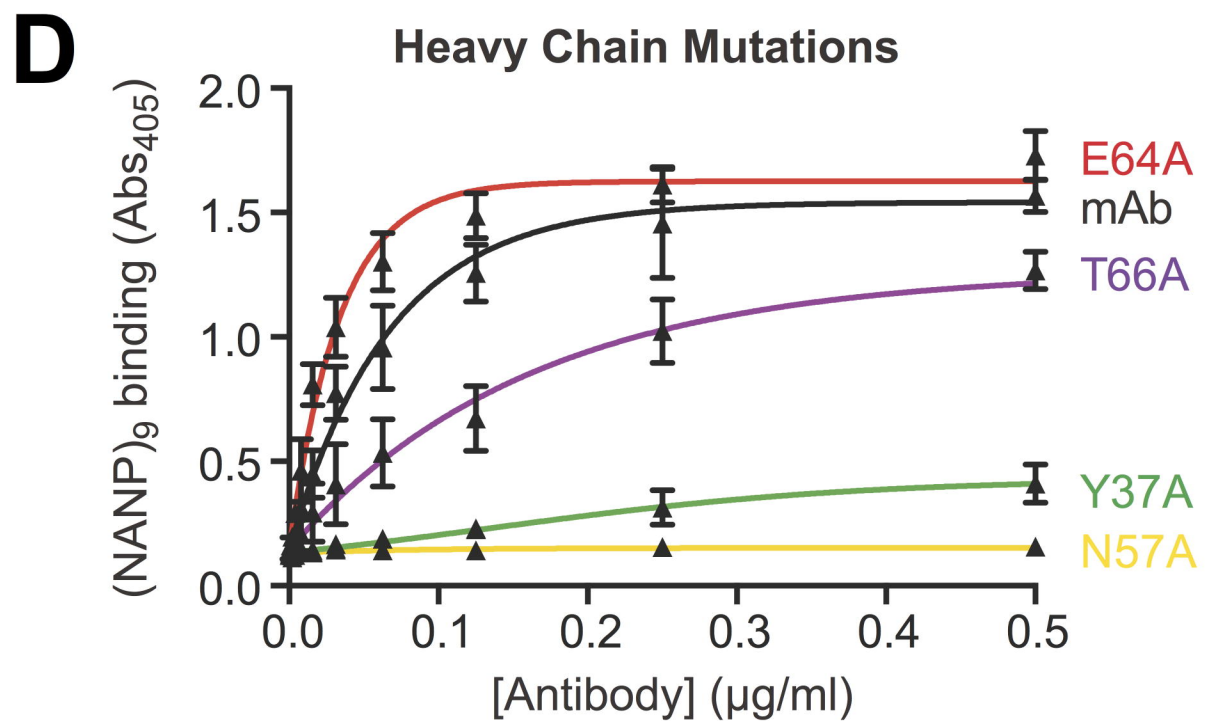
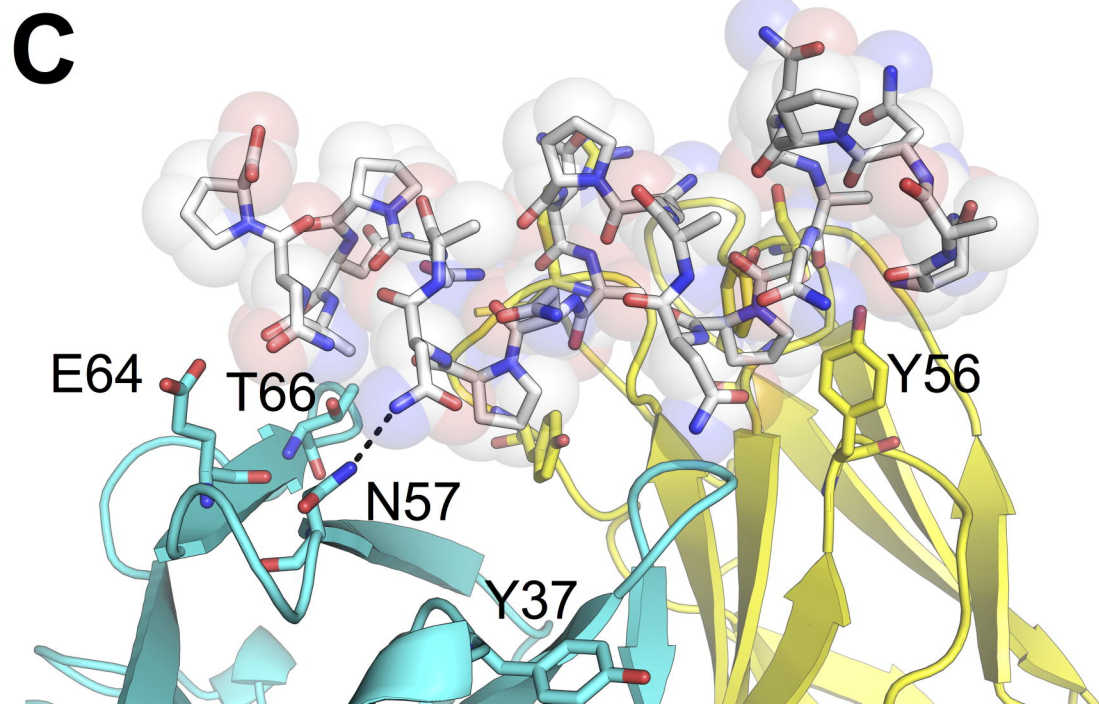
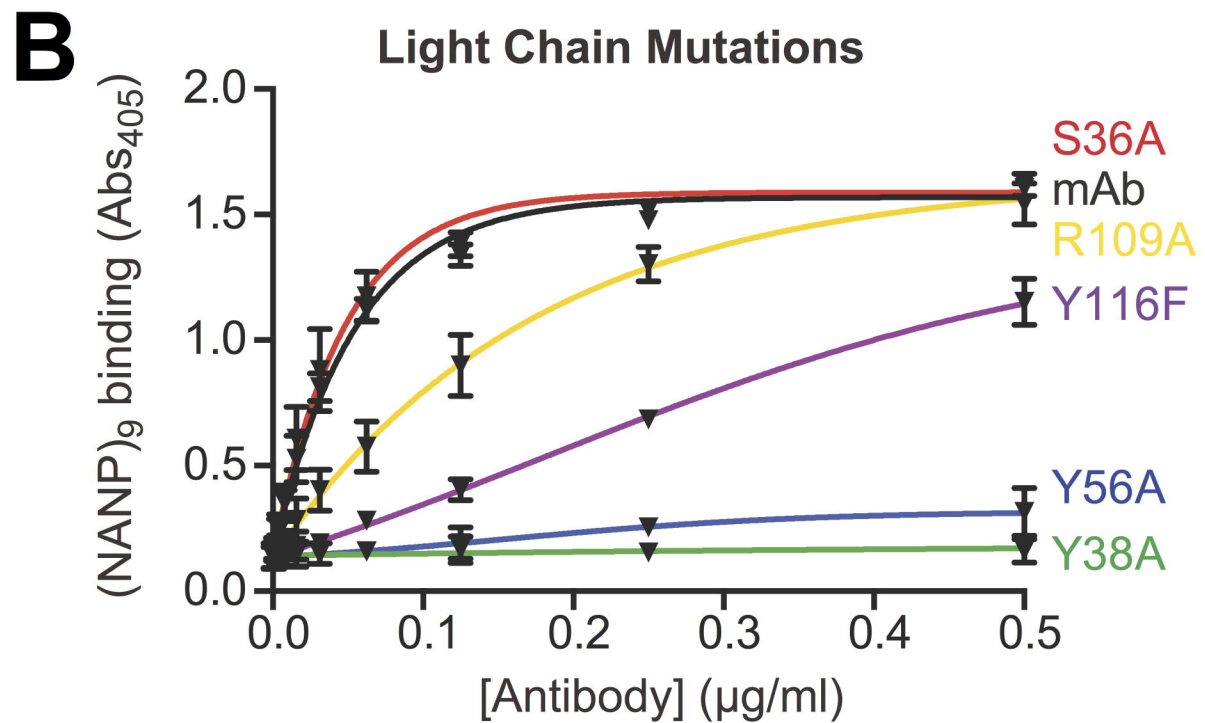
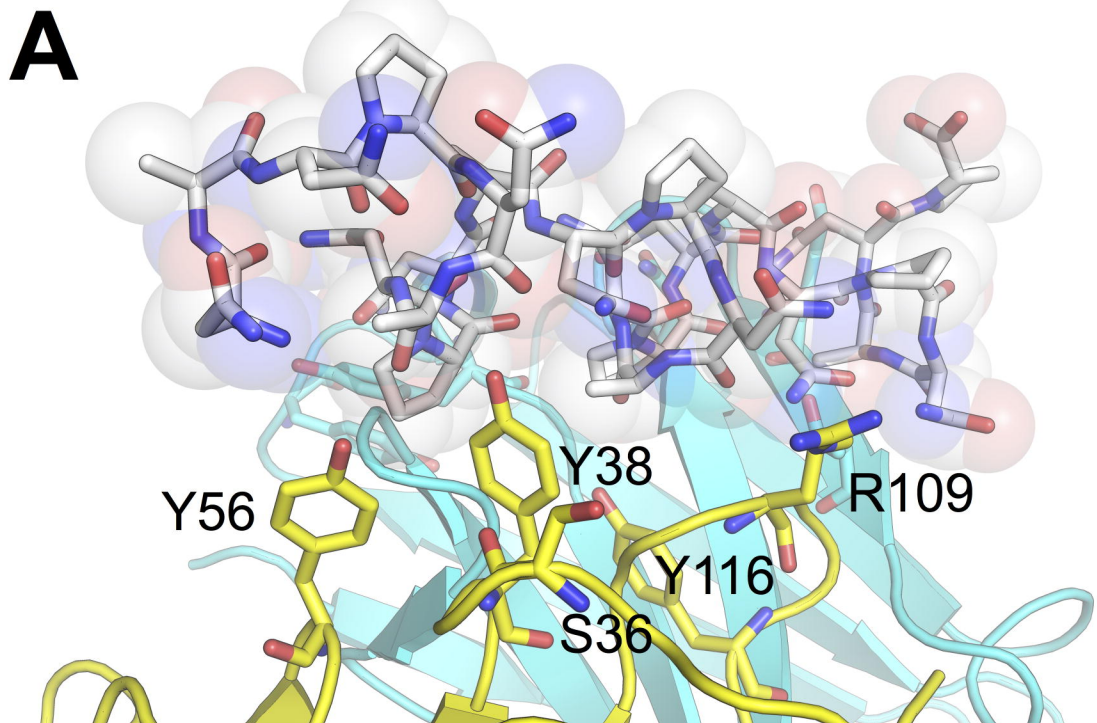
850

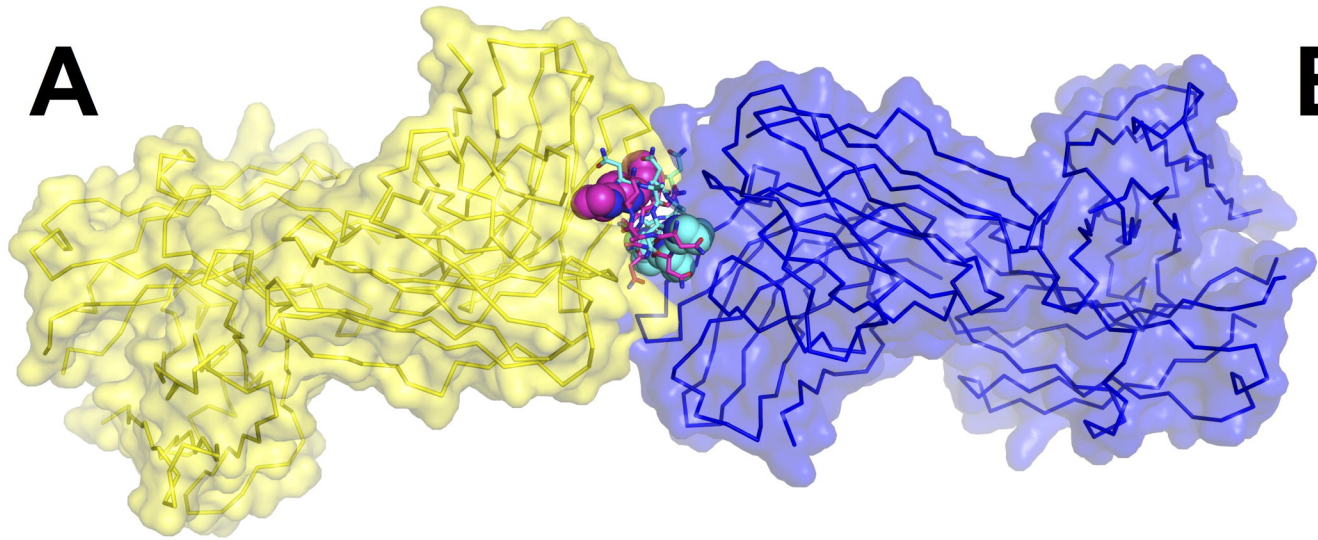
851 **Fig 7: CSP-binding antibodies undergo somatic hypermutation and affinity**

852 **maturation** (A) Violin plots showing the number of mutations per read from bulk B
853 cells from 3 individual naïve mice and sorted (NANP)_n specific B cells from
854 sporozoite immunized mice (B) Skyscraper plots showing the location of mutations
855 away from germline in the IGKV1-110 gene in a naïve mouse and in sorted (NANP)_n
856 specific cells in three sporozoite immunized mice. (C) ELISA binding to the (NANP)₉
857 peptide of recombinant antibodies corresponding to the 2A10 mAb, the predicted
858 germline precursor, and hybrid antibodies containing the 2A10 heavy chain (mHC)
859 paired with the germline light chain (gLC) and the 2010 light chain (mLC) paired
860 with germline heavy chain (gHC). (D) Predicted mutations in the gLC were
861 introduced to the germline precursor and their effect on binding to (NANP)₉ measured
862 by ELISA (E) Predicted mutations in the gHC were introduced to hybrid antibodies
863 consisting of the mLC and the gHC heavy chain and their effect on binding to
864 (NANP)₉ measured by ELISA.



A**B****C**



A**B**